

Revisiting DDIM Inversion for Controlling Defect Generation by Disentangling the Background

Youngjae Cho

Gwangyeol Kim

Sirojbek Safarov
AiV Co.

Seongdeok Bang

Jaewoo Park

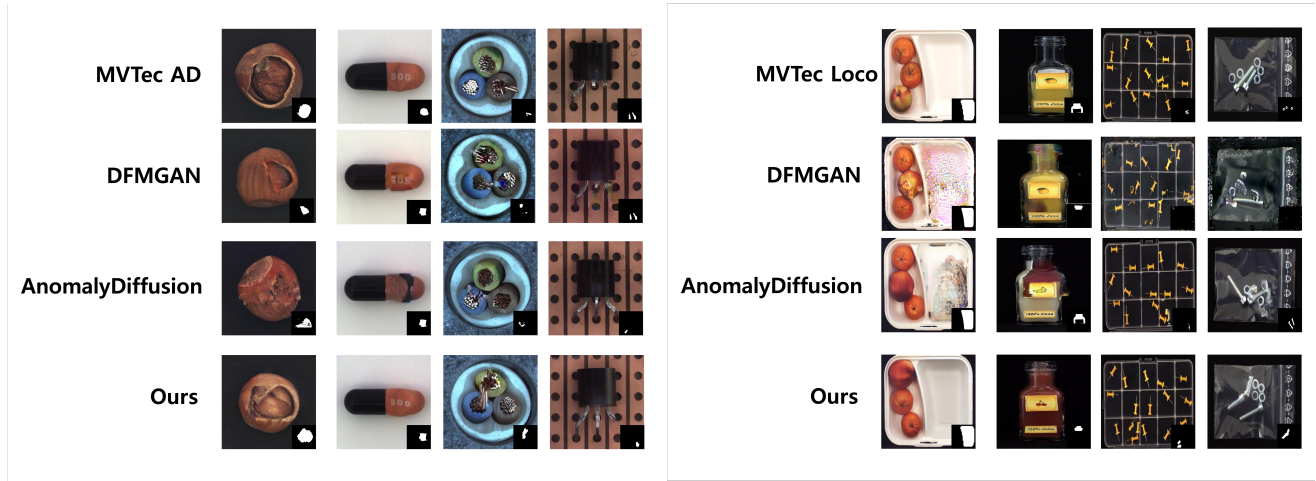


Figure 1. Left image is a comparison between ours and baselines for MVTec AD. Right image is a comparison between ours and baselines for MVTec Loco

Abstract

In anomaly detection, the scarcity of anomalous data compared to normal data poses a challenge in effectively utilizing deep neural network representations to identify anomalous features. From a data-centric perspective, generative models can solve this data imbalance issue by synthesizing anomaly datasets. Although previous research tried to enhance the controllability and quality of generating defects, they do not consider the relation between background and defect. Since the defect depends on the object’s background (i.e., the normal part of an object), training only the defect area cannot utilize the background information, and even generation can be biased depending on the mask information. In addition, controlling logical anomalies should consider the dependency between background and defect areas (e.g., orange colored defect on a orange juice bottle). In this paper, our paper proposes modeling a relationship between the background and defect, where background affects denoising defects; however, the reverse is not. We introduce the regularizing term to disentangle denoising background from defects. From the disentanglement

loss, we rethink defect generation with DDIM Inversion, where we generate the defect on the target normal image. Additionally, we theoretically prove that our methodology can generate a defect on the target normal image with an invariant background. We demonstrate our synthetic data is realistic and effective in several experiments.

1. Introduction

Data scarcity presents a significant challenge in industrial anomaly detection, as imbalanced datasets can lead to overfitting in deep neural networks, damaging inspection performance. Limited labeled training examples introduce model bias, preventing the detection model from effectively generalizing to unseen anomalies. Recent unsupervised anomaly detection approaches [5, 17, 23] mitigate the imbalance issue by avoiding reliance on anomaly instances during training. However, these methods may struggle when the backbone model experiences distribution shifts in feature space, making it difficult to distinguish normal and anomalous features. Additionally, they often fall short in detecting fine-grained anomalies at the pixel level.

Recent research on defect generation aims to address data scarcity through a data-centric approach, synthesizing anomaly data to train on augmented samples. GAN-based methods [6] generate realistic synthetic anomaly data from limited examples, improving model performance on rare anomalies; however, they lack control over defect location, often transforming normal regions into anomalies unintentionally. Diffusion-based methods [10] improve control by specifying defect locations and blending normal latent backgrounds with synthetic defect latents. While these personalization techniques enable defect placement on object backgrounds, some challenges remain unaddressed.

First, focusing solely on controllability with masks can compromise the quality of generation. Since the defect’s appearance is dependent on the background of the target image, using a misleading mask may result in the generation of a biased anomaly that does not align with the data distribution. For example, defects should not appear outside the objects themselves. Additionally, defects should vary based on the texture of the background and the location of the target mask such as Figure 3. Generating logical anomalies, in particular, becomes challenging without accounting for the relationship between the defect and the background, especially when compared to generating structural anomalies, which are easier to control.

Secondly, overfitting to few-shot anomaly instances can lead to biased generation, where controllable defect generation may fail when encountering unseen backgrounds. Since anomaly instances consist of both foreground (defect) and background, it is crucial to model the relationship between these two components to mitigate overfitting issues. This consideration helps ensure that the model can generate defects effectively, avoiding the transfer of inadequate feature of the defect.

To address the issues mentioned above, we propose modeling the relationship between the defect and background to achieve both high-quality and controllable defect generation. Our work suggests the disentanglement loss function for generating faithful defects on the target normal instances. Our formulation ensures independence from defect to background, allowing the denoising process for defects to proceed without affecting the background’s denoising process. At the same time, the background influences the defect area’s denoising process, enhancing defect generation by reducing reliance on the mask information. In addition, we propose the inference strategy to generate defect on the target normal latent, where we apply DDIM Inversion to the normal latent and generate defects on the background. We theoretically show that we can initialize anomaly latent by noising the target area of inversed normal latent while reconstructing its background. To sum up, we make the following contributions.

- We introduce a regularization loss that generates defect based on background but without influencing background generation with defect characteristics.
- We theoretically show that our loss formulation can inverse anomaly latent given the latent of background under the DDIM inversion and maintain the background reconstruction.
- We demonstrate that our methodology can generate faithful and diverse generations and effectively mitigate data scarcity for detecting structure and logical anomalies.

2. Background

2.1. Industrial anomaly detection

Industrial anomaly detection (IAD) has seen significant progress, transitioning from traditional methods reliant on labeled data to more advanced machine learning and computer vision approaches. By leveraging pretrained models to extract normal features, unsupervised anomaly detection methods focus on identifying anomalous regions in products [3–5, 17, 23]. Memory-based approaches [3, 4, 23] store normal feature representations and calculate similarity scores to pinpoint anomalous regions. However, since unsupervised methods do not incorporate anomalous features during training, accurately detecting defect areas in anomaly instances remains challenging. As a result, supervised or semi-supervised learning methods remain highly effective for identifying fine-grained defect areas at the pixel level, especially when sufficient anomaly instances are available for training.

2.2. Defect generation

Collecting sufficient anomalous data is challenging due to the time-consuming nature and high annotation costs involved. To address this scarcity, data augmentation and generation methods have been developed. Cut-Paste [14] employs pixel-level data augmentation, while Crop-Paste [16] focuses on feature-level augmentation to help the model learn discriminative features between normal and anomalous data. However, since these augmentation-based methods do not model distributions of anomalies, generating a faithful defect dataset remains difficult.

In the DFMGAN [6] paper, the authors leverage StyleGAN [12] to generate defects from a limited number of anomalous data. While they also incorporate normal data to guide defect generation, their approach lacks the ability to control defect generation on unseen target normal data. In contrast, AnomalyDiffusion [10] addresses this by training a Text-to-Image diffusion model to control defect generation on target normal images. However, their method does not train the diffusion process to account for the background

of anomalous data, meaning that defect generation does not consider the relationship between the defect and the target normal background. Since some defects are dependent on the background, it is crucial to model the interaction between the background and defect to generate more faithful and contextually accurate defects.

2.3. Diffusion model

Since the advent of diffusion models [9, 26], text-to-image (T2I) models [20] that control image generation through text has been developed. The denoising network ϵ_θ is conditioned on text embedding C , where text embedding controls the output with cross-attention. Latent variable, z_t is injected by Gaussian noise ϵ from the z_0 as follows [9]:

$$z_t = \sqrt{\alpha_t}z_0 + \sqrt{1 - \alpha_t}\epsilon, \text{ where } \epsilon \sim \mathcal{N}(0, I) \quad (1)$$

From noising the latent in Eq.1, the network is trained to minimize the following loss between random noise ϵ and the noise prediction $\epsilon_\theta(z_t, t, C)$:

$$\min_{\theta} E_{z_0, \epsilon \sim \mathcal{N}(0, I), t \sim \text{Uniform}(1, T)} \|\epsilon - \epsilon_\theta(z_t, t, C)\|_2^2 \quad (2)$$

2.4. DDIM Inversion

By the DDIM Sampling [25], we can denoise the noise with non-Markovian deterministic diffusion process as follows:

$$\begin{aligned} z_{t-1} &= \sqrt{\alpha_{t-1}} \left(\frac{z_t - \sqrt{1 - \alpha_t} \cdot \epsilon_\theta(z_t, t, C)}{\sqrt{\alpha_t}} \right) \\ &\quad + \sqrt{1 - \alpha_{t-1}} \cdot \epsilon_\theta(z_t, t, C) \\ &= \sqrt{\alpha_{t-1}} \left[\sqrt{\frac{1}{\alpha_t}} z_t + \left(\sqrt{\frac{1}{\alpha_{t-1}} - 1} - \sqrt{\frac{1}{\alpha_t} - 1} \right) \right. \\ &\quad \left. \cdot \epsilon_\theta(z_t, t, C) \right] \end{aligned} \quad (3)$$

With approximating to ODE path, we can reverse the denoising steps (i.e., DDIM Inversion), where some initial \tilde{z}_T can be noised from the z_0 as follows:

$$\begin{aligned} \tilde{z}_t &= \sqrt{\alpha_t} \left[\sqrt{\frac{1}{\alpha_{t-1}}} \tilde{z}_{t-1} + \left(\sqrt{\frac{1}{\alpha_t} - 1} - \sqrt{\frac{1}{\alpha_{t-1}} - 1} \right) \right. \\ &\quad \left. \cdot \epsilon_\theta(\tilde{z}_{t-1}, t - 1, C) \right] \end{aligned} \quad (4)$$

Especially, from the DDIM Inversion [25], editing of target images is enabled with changing text embeddings [7, 18]. Furthermore, target images can be translated to source image concepts via controlling cross-attention. In this paper, we utilize the DDIM Inversion to personalize the target normal images and generate the defect in the target area.

3. Method

3.1. Loss formulation

As discussed earlier, our objective is to model the relationship between defect and background in order to generate more accurate defect representations on normal images. In the U-Net architecture, attention mechanisms facilitate interaction between defect and background regions, effectively reducing random noise. While defects may vary depending on the background context, the background itself should remain unaffected by defect generation. To decouple the influence of defects on the background, we propose the following loss formulation with masked noising strategy.

$$\begin{aligned} \mathcal{L}(\theta) &:= E_{z_0, \epsilon, t} \left\| \underbrace{m \odot (\epsilon - \epsilon_\theta(z_t, t, C_1))}_{\text{Matching Loss}} \right\|_2^2 \\ &\quad + \left\| \underbrace{(1 - m) \odot (\epsilon - \epsilon_\theta(z_t^m, t, C_2))}_{\text{Regularizer}} \right\|_2^2 \\ &= \|\epsilon - m \odot \epsilon_\theta(z_t, t, C_1) - (1 - m) \odot \epsilon_\theta(z_t^m, t, C_2)\|_2^2 \end{aligned} \quad (5)$$

We suppose that text embedding, $C_1 = [C_{def}, C_{bg}]$, $C_2 = [C_m, C_{bg}]$ and we mask its cross-attention with source mask, m in the training dataset, where the C_{def} , C_m attentions on masked area and C_{bg} attentions on another area like Figure. 2. Masked latent is defined as masking the anomaly latent as follows: $z_0^m := (1 - m) \odot z_0$, $z_0 \sim p(z_0)$. From Eq.1, we inject the noise to each latent as follows.

$$z_t = \sqrt{\alpha_t}z_0 + \sqrt{1 - \alpha_t}\epsilon \quad (6)$$

$$z_t^m = \sqrt{\alpha_t}z_0^m + \sqrt{1 - \alpha_t}(1 - m) \odot \epsilon \quad (7)$$

In Eq.5, minimizing *Matching Loss* denoises that defect area of z_t with considering the noised background area. Since $(1 - m) \odot z_t = z_t^m$ is satisfied for all t , minimizing *Regularizer* term denoises the background area of z_t , where the denoising process of the background area of z_t is independent on the defect area of z_t . We prove this statement in Lemma 1.

Lemma 1. *Suppose that $\mathcal{L}(\theta^*) = 0$, then background of z_t is reconstructed as follows:*

$$(1 - m) \odot z_0 = (1 - m) \odot \sqrt{\frac{1}{\alpha_t}} [z_t^m - \sqrt{1 - \alpha_t} \epsilon_\theta(z_t^m, t, C_2)]$$

According to Lemma 1, it is possible to reconstruct the background without requiring information about the defect area. As a result, the model can produce a variety of defects while generating the same background. The proof of Lemma 1 is provided in Appendix.

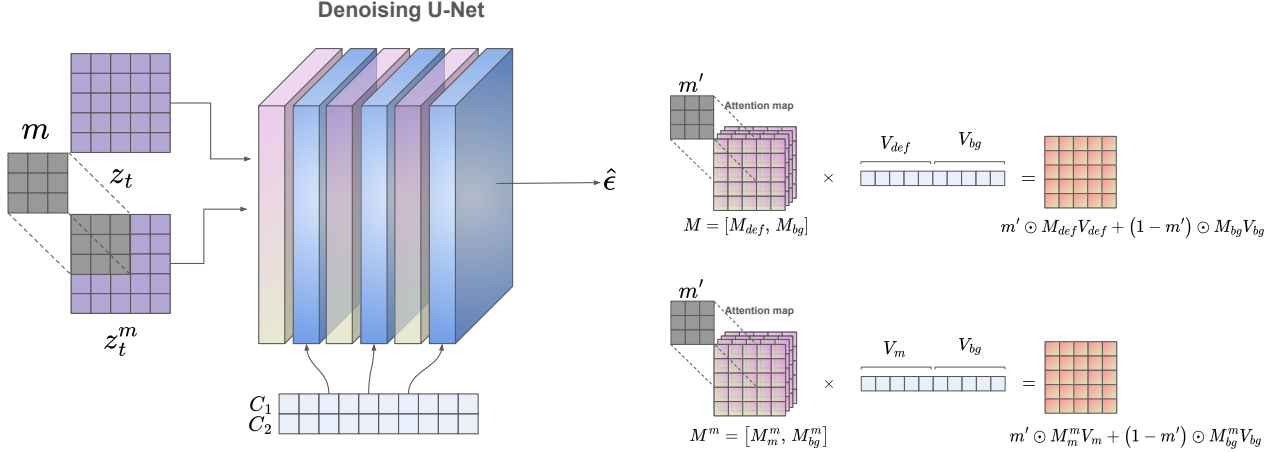


Figure 2. Framework of our defect generation. The left image is the overview of the denoising process for latent in U-Net. The right image is the details of cross attention process in U-Net, where we use the masking strategy for disentangling each text embedding.

3.2. DDIM Inversion for generating synthetic data

To effectively control the defect on target normal latent, z_0^{normal} , it is essential to identify the initial state of the target normal latent representation. To achieve this, we employ DDIM Inversion on normal images using the target masks. This approach allows us to accurately initialize the latent space for normal images, enabling precise control over defect generation. From Eq.4, we reverse the denoising steps of $z_0^m := (1 - m) \odot z_0^{normal}$, $z_0 \sim p(z_0^{normal})$ as follows:

$$\begin{aligned} \tilde{z}_t^m = & \sqrt{\alpha_t} \left[\sqrt{\frac{1}{\alpha_{t-1}}} \tilde{z}_{t-1}^m + (1 - m) \odot \left(\sqrt{\frac{1}{\alpha_t} - 1} \right. \right. \\ & \left. \left. - \sqrt{\frac{1}{\alpha_{t-1}} - 1} \right) \epsilon_{\theta}(\tilde{z}_{t-1}^m, t - 1, C_2) \right] \end{aligned} \quad (8)$$

After reversing the latent, \tilde{z}_T^m , the denoising path should generate the defect on the mask area. To guarantee defect generation on the target mask, we present the following theorem to demonstrate that the standard initialization strategy works. We prove Theorem 1 in Appendix.

Theorem 1. *Suppose that $\mathcal{L}(\theta^*) = 0$ and $\alpha_{t-1} > \alpha_t$ for all t , then $\lim_{\alpha_t \rightarrow 0} \tilde{z}_t - \tilde{z}_t^m = m \odot \epsilon$, $\epsilon \sim \mathcal{N}(0, I)$*

Suppose that Theorem 1, we randomly initialized the latent, $z_T^* = \tilde{z}_T^m + m \odot \epsilon$, where $\epsilon \sim \mathcal{N}(0, I)$. From Eq.9, denoising z_t^* generates the defect on the mask area affected by the denoised background part of latent, z_t^m .

$$\begin{aligned} z_{t-1}^* = & \sqrt{\alpha_{t-1}} \left[\sqrt{\frac{1}{\alpha_t}} z_t^* + \left(\sqrt{\frac{1}{\alpha_{t-1}} - 1} - \sqrt{\frac{1}{\alpha_t} - 1} \right) \right. \\ & \left. \times ((1 - m) \odot \epsilon_{\theta}(z_t^m, t, C_2) + m \odot \epsilon_{\theta}(z_t^*, t, C_1)) \right] \end{aligned} \quad (9)$$

Although we initialize the masked area with random noise, Proposition 1 proves that denoising z_t^* maintains the DDIM-Inversion gap, where we kept the background of the target normal image.

Proposition 1. *Suppose that $\mathcal{L}(\theta^*) = 0$ and DDIM Inversion Path follows Eq.8 then $\|(1 - m) \odot (z_t^m - \tilde{z}_t^m)\|_2^2 = \|(1 - m) \odot (z_t^* - \tilde{z}_t^m)\|_2^2$*

From Proposition 1, defect generation on target mask still does not affect the denoising of background after DDIM Inversion. We prove Proposition 1 in Appendix.

3.3. Masking attention and refinement of mask

3.3.1. Masking attention strategy

As previously discussed, our objective is to control defect generation under the disentangled background, where its denoising process is independent of another area of latent. In the Text-to-Image (T2I) model, U-Net is designed with self-attention and cross-attention mechanisms, where cross-attention facilitates interaction between text embeddings and latent features.

To disentangle each text embedding, we define masked cross-attentions of z_t and z_t^m inspired by [19]. In the process of cross-attention, m' is resized mask and each attention map is defined as follows: $M := [M_{def}, M_{bg}] = [\text{softmax}(\frac{QK_{def}^T}{\tau}), \text{softmax}(\frac{QK_{bg}^T}{\tau})]$ and $M^m :=$

$[M_m^m, M_{bg}^m] = [\text{softmax}(\frac{Q^m K_m^T}{\tau}), \text{softmax}(\frac{Q^m K_{bg}^T}{\tau})]$, where Q and Q^m are from query vectors from z_t and z_t^m , respectively. K_{def} , K_{bg} , and K_m are the key vectors from the text encoder embeddings C_{def} , C_{bg} , and C_m , respectively. Then, the masked cross-attention is given by

$$\text{Attn}^C(z_t, C_1) = m' \odot M_{def} V_{def} + (1 - m') \odot M_{bg} V_{bg} \quad (10)$$

$$\text{Attn}^C(z_t^m, C_2) = m' \odot M_m^m V_m + (1 - m') \odot M_{bg}^m V_{bg} \quad (11)$$

with value vectors V_{def} , V_{bg} , and V_m given like the key vectors.

Although we do not directly mask the self-attention layer, our formulation enables masked self-attention for the background part due to $m \odot z_t^m = 0$ and $z_t^m = (1 - m) \odot z_t^m$. Namely, the following masked self-attention holds:

$$\begin{aligned} \text{Attn}^S(z_t^m) &= \text{Softmax}\left(\frac{\hat{Q}^m \hat{K}^{mT}}{\tau}\right) \hat{V}^m \\ &= \text{Softmax}\left(\frac{\hat{Q}^m \hat{K}^{mT}}{\tau}\right) (1 - m') \odot \hat{V}^m \\ &= (1 - m') \odot \text{Attn}^S(z_t^m) \end{aligned} \quad (12)$$

Here, \hat{Q}^m , \hat{K}^m , \hat{V}^m are the query, key, values on the self-attention layer from the masked latent z_t^m .

Since $(1 - m) \odot \epsilon_\theta(z_t^m, t, C_2)$ denoises that the background of z_t , Eq.12 shows that its denoising step only depends on the background of z_t . The details will be given in Supplementary

3.3.2. Refining target mask with attention

During inference, we guide defect generation within the target mask m ; however, its generation may not be filled within the target mask. This occurs because background latents can influence the defect region, occasionally incorporating background elements into the generated defect. To address this, we refine the target mask to ensure a more precise defect localization. This refined mask is then used to construct a robust training dataset for anomaly detection.

After DDIM Inversion to \tilde{z}_T^* in Eq. 9, we can save cross-attention map of $\epsilon_\theta(z_t^*, C_2)$, where text embedding of C_{def} can refine the target mask m with its attention map as Eq.13. Since the resolution of the cross-attention map is less than or equal to the resolution of latent, we should upscale the attention map to refine the target mask. *Resize* means that the upscaling algorithm such as the Bilinear interpolation.

$$\begin{cases} m_{i,j}^* = 1, & \text{if } \text{Resize}\left(m' \odot \text{Softmax}\left(\frac{Q K_{def}^T}{\tau}\right)\right)_{i,j} \geq \frac{1}{2} \\ m_{i,j}^* = 0, & \text{if } \text{Resize}\left(m' \odot \text{Softmax}\left(\frac{Q K_{def}^T}{\tau}\right)\right)_{i,j} < \frac{1}{2} \end{cases} \quad (13)$$

Algorithm 1 indicates our defect generation process, where synthetic data would be used as a training dataset for downstream anomaly detection tasks.

Algorithm 1 Training and Inference

- 1: **Input:** Anomaly Dataset $\{z_0, m\} \sim \{p(z_0), p(m)\}$, Normal Dataset $\{z_0^{normal}, m\} \sim \{p(z_0^{normal}), p(m)\}$ U-Net parameter θ , Context vector C_1, C_2
 - 2: **while** not converged **do** ▷ Training
 - 3: Compute $\mathcal{L}(\theta)$ based on $\{z_0, m\}$
 - 4: Update $\theta \leftarrow \theta - h \nabla_\theta \mathcal{L}(\theta)$
 - 5: **end while**
 - 6: DDIM Inversion for $z_0^m := (1 - m) \odot z_0^{normal}$ by Eq. 8 ▷ Inference
 - 7: DDIM Sampling for z_T^* by Eq. 9
 - 8: Mask Refinement for m^* by Eq. 13
 - 9: Return z_0^*, m^*
-

4. Experiment

4.1. Experimental settings

Dataset In this paper, we conduct our experiments on industrial anomaly detection benchmark datasets: MVTec-AD [1] and MVTec-LoCo [2]. Each dataset includes anomaly instances in the test set, while the training set contains only normal instances. To train the generative model on these anomaly instances, we split each anomaly dataset into two folds: one fold is used for training the generative model, and the other for evaluating inspection performance in anomaly detection. For unsupervised settings, we exclude anomaly instances from training, as unsupervised methods do not learn from anomaly data.

Details of experiments We utilize the Stable Diffusion [21] for fine-tuning anomaly dataset with 500 iterations, where each model is trained on the defect type of objects. We only trained the U-Net part of Stable Diffusion followed by Dreambooth [24] and inferred the sample with DDIM sampler [25] with 50-time steps.

Baseline We compared our methodology with other defect generation-based methodologies; DFMGAN [6] and Anomalydiffusion [10], where each setting is identical in their papers. In addition, we compared ours with Unsupervised-based anomaly detection; RD4AD [5], Patchcore [23], and SimpleNet [17].

4.2. Synthetic Data Quality

For comparing generation quality between ours and other baselines, we measure FID score [8] and LPIPS [27] for each category in MVTec-AD and MVTec-LoCo, and use 100 synthetic images per each categories from each generative model trained on split folds in each benchmark

Table 1. Result of FID Score and LPIPS in MVTec-AD. Bold means the best performance and underline means the second-best performance.

Category	DFMGAN		AnomalyDiffusion		Ours	
	FID↓	LPIPS↓	FID↓	LPIPS↓	FID↓	LPIPS↓
Bottle	77.23	0.176	<u>57.09</u>	<u>0.150</u>	52.23	0.143
Cable	199.22	0.461	<u>136.00</u>	<u>0.402</u>	125.40	0.396
Capsule	58.19	0.191	40.63	0.142	28.21	<u>0.143</u>
Carpet	44.56	0.273	64.29	0.273	53.92	0.277
Grid	186.63	<u>0.444</u>	<u>135.10</u>	0.451	131.38	0.433
Hazelnut	89.40	0.305	<u>82.37</u>	<u>0.260</u>	69.20	0.253
Leather	130.28	0.372	161.29	0.346	<u>141.34</u>	<u>0.360</u>
Metal Nut	<u>85.89</u>	0.357	97.50	<u>0.332</u>	76.58	0.315
Pill	177.87	0.280	<u>67.73</u>	<u>0.202</u>	56.85	0.194
Screw	34.46	<u>0.353</u>	39.61	0.338	<u>36.52</u>	0.338
Tile	232.08	0.519	<u>205.33</u>	0.509	134.77	<u>0.510</u>
Toothbrush	98.10	0.246	<u>57.63</u>	<u>0.159</u>	49.94	0.158
Transistor	132.70	0.377	<u>99.36</u>	<u>0.338</u>	92.41	0.328
Wood	211.87	0.398	<u>158.58</u>	<u>0.357</u>	121.45	0.353
Zipper	116.46	0.264	<u>98.02</u>	<u>0.255</u>	91.09	0.249
Average	132.96	0.334	<u>104.36</u>	<u>0.301</u>	88.17	0.297

datasets. Table 1 demonstrates our methodology can generate more realistic and diverse structure anomaly images, where our method overall outperforms the baseline. In addition, Table 3 shows that our methodology outperforms in logical anomalies, where our model generates the defect considering the background.

Since DFMGAN does not control the generation given the target mask, its generation is not as diverse as diffusion-based methods and its generation quality is low overall. Although Anomalydiffusion [10] is also diffusion-based

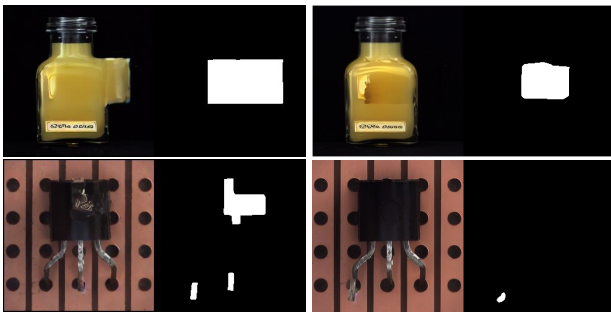


Figure 3. Visualization of synthetic instances given identical target mask. The left side is from Anomalydiffusion and the right side is from ours. The right side mask is refined mask from Eq. 13.

method, it sometimes generates some unrealistic defects depending on the target mask mentioned previously. Figure 3 shows that Anomalydiffusion generates the defects given target mask, but its generation can be located out of objects. Since they usually generate fully filled defects in the masked area, their generation could be low-quality, where

its generation can be bias for anomaly detection training. Further generations are shown in Appendix.

4.3. Anomaly Detection

4.3.1. Quantitative Analysis

To demonstrate our synthetic methodology’s effectiveness in anomaly detection, we utilized the generated dataset for training a segmentation backbone. In this experiment, we trained naive U-Net [22] with both real and synthetic defect datasets. We use normal samples in training and 100 defect instances per defect type for 200 epochs followed by the framework of Anomalydiffusion [10].

For a fair comparison, we report the average performance of each split fold, where a test set of one fold is used as a train set of another fold. Furthermore, we also compare our method with the Unsupervised-based anomaly detection (UAD) baselines. To fairly report the performances of UAD, we limit the normal train set to be same with synthetic-based methods and report detection performances of each fold. The other settings of UAD baselines are identical to their origin paper.

Table 2 demonstrates that our synthetic dataset enhances both detection and segmentation performances of anomaly detection in MVTec-AD, where we report the AUROC, AP (Average Precision), and F1 max score for image and pixel level. Additionally, we report the PRO score to consider the inspection performance of tiny defects. Although image-level metrics of unsupervised-based methods attain higher scores than other synthetic-based methods, our method is comparable and even better in pixel-level performances. Furthermore, we conducted anomaly detection in the MVTec-LoCo, where we reported the performance of logical anomalies. Table 2 shows that our synthetic strategy outperforms other baselines in both image and pixel levels. Since unsupervised-based anomaly detection exploits the normal features, the detection performance shows degradation compared to the supervised setting. Although our methodology is based on the diffusion model, the performance demonstrates that our generation facilitates more robust training by reducing logically incorrect generations, as illustrated in Figure 3, where it demonstrates that the quality of generation is related to the performance of anomaly detection.

4.3.2. Qualitative Analysis

We extend our anomaly detection experiment to analyze the effect of the synthetic datasets from the perspective of the training loss landscape [15], where we visualize the loss landscape of each normal and anomaly training dataset without synthetic instances in Figure. 4. According to several studies [11, 13] indicating that attaining a loss flat minima is closely related to model generalization, our methodology enables more robust learning for unseen anomalies.

Table 2. Result of anomaly detection in benchmark datasets. We ensure a fair comparison by keeping the dataset configuration of the unsupervised baselines the same as for the synthetic-based baselines, except for the training dataset. Notably, the synthetic-based baselines use supervised settings, where their training datasets include anomaly instances. For MVTec-Loco, we only conduct experiments for logical anomaly class. Bold text indicates the best performance, and underlined text highlights the second-best performance.

Unsupervised-based							
Method	Image-level			Pixel-level			
	AUROC	AP	F1	AUROC	AP	F1	AUPRO
RD4AD	98.0	99.0	97.8	97.8	56.7	59.9	93.9
Patchcore	<u>99.1</u>	99.8	98.6	98.1	57.3	59.9	93.0
SimpleNet	99.3	<u>99.7</u>	98.6	97.7	55.1	57.4	91.4
Synthetic-based							
DFMGAN	98.0	99.4	97.6	96.2	74.0	71.1	88.6
Anomalydiffusion	98.0	99.3	<u>97.9</u>	<u>97.9</u>	<u>77.1</u>	<u>73.4</u>	91.7
Ours	99.3	99.8	98.6	98.1	78.9	74.2	<u>93.6</u>

(a) MVTec-AD

Unsupervised-based							
Method	Image-level			Pixel-level			
	AUROC	AP	F1	AUROC	AP	F1	AUPRO
RD4AD	70.2	63.6	61.8	72.4	21.6	25.4	57.6
Patchcore	69.1	62.4	60.4	70.6	33.3	33.4	55.2
SimpleNet	74.0	67.3	62.8	71.5	35.8	36.8	53.4
Synthetic-based							
DFMGAN	84.7	79.8	77.0	88.6	51.8	55.1	78.3
Anomalydiffusion	<u>85.8</u>	<u>81.9</u>	<u>78.5</u>	<u>91.4</u>	<u>59.0</u>	<u>61.2</u>	<u>80.2</u>
Ours	89.9	87.1	84.0	95.3	79.8	78.2	84.2

(b) MVTec-Loco

Table 3. Result of FID Score and LPIPS in MVTec-Loco. Bold means the best performance and underline means the second-best performance.

Category	DFMGAN		AnomalyDiffusion		Ours	
	FID↓	LPIPS↓	FID↓	LPIPS↓	FID↓	LPIPS↓
Breakfast Box	178.61	0.419	<u>119.42</u>	<u>0.353</u>	84.90	0.316
Screw Bag	245.83	0.523	<u>116.19</u>	<u>0.368</u>	104.62	0.367
Juice Bottle	<u>71.49</u>	0.344	76.17	<u>0.280</u>	44.94	0.246
Splicing Connectors	90.87	0.402	125.71	0.497	<u>114.61</u>	<u>0.483</u>
Pushpins	162.20	0.471	<u>56.05</u>	<u>0.385</u>	44.53	0.382
Average	145.19	0.432	<u>102.92</u>	<u>0.376</u>	79.49	0.359

Especially, loss landscape of anomaly samples is flatter than other baselines, which demonstrates our better performance given anomalies in both image and pixel levels.

4.3.3. Ablation Study

Effect of Regularizer in Eq. 5 To demonstrate our loss formulation effective in generating a faithful synthetic dataset, we compared our loss function with naive loss L'

defined as Eq.2. After minimizing L' , we denoise the random noise $z_T \sim \mathcal{N}(0, I)$ by DDIM sampler. Table 4 shows that modeling the relation between background and defect can facilitate diversity and fidelity of generation. In addition, initializing the latent via DDIM inversion is more appropriate than random initialization in the few-shot training scenario.

Table 4. Ablation study for loss function. We compare our loss formulation with naive matching loss and report the sampling quality of the synthetic dataset in MVTec-AD.

Category	$L'(\theta)$		$L(\theta)$	
	FID↓	LPIPS↓	FID↓	LPIPS↓
Capsule	117.25	0.294	28.21	0.143
Hazelnut	134.27	0.357	69.20	0.253
Transistor	162.84	0.312	92.41	0.328
Wood	196.76	0.369	121.45	0.353
Average	152.78	0.333	77.82	0.269

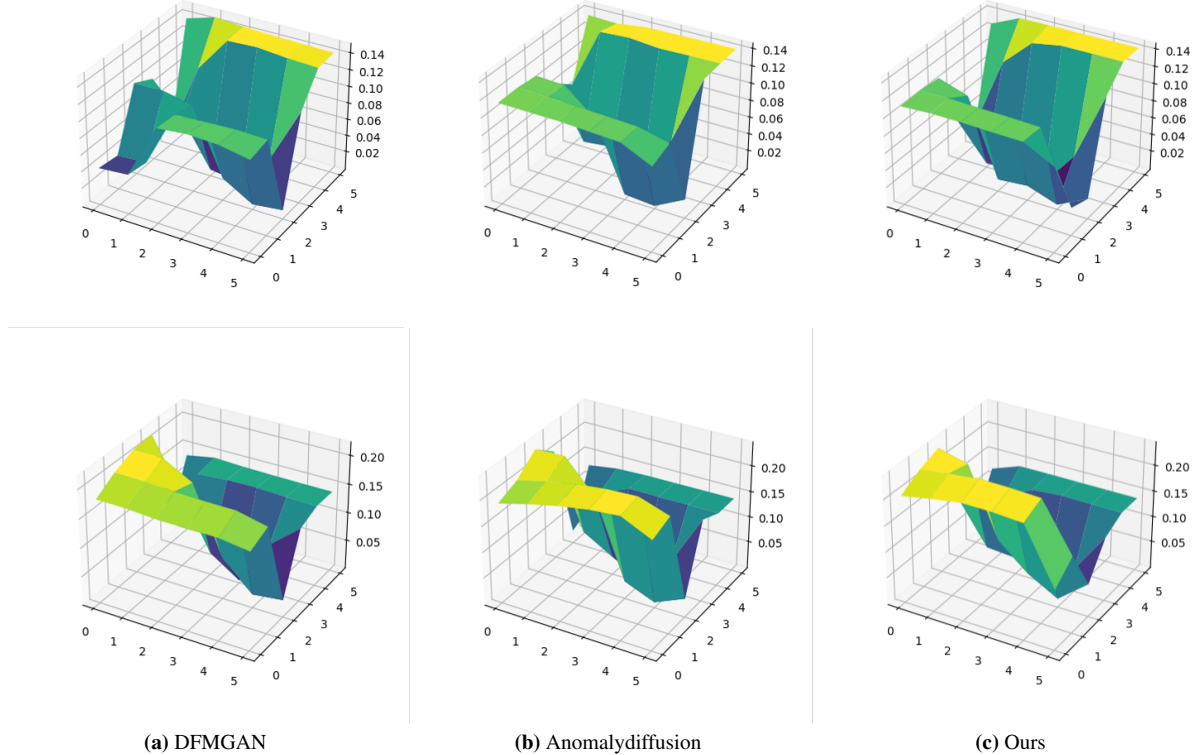


Figure 4. Comparison of training loss landscape between ours and baselines in MVTec-AD. The first row is the loss landscapes of training normal sample. The second row is the loss landscapes of training anomaly sample except for synthetic anomalies.

Effect of Mask Refinement in Eq. 13 As shown in Figure 3, our defect generation is affected by background information given an unseen mask and refines the target mask with cross-attention in Eq. 13. To demonstrate the mask refinement trick, we conduct an ablation study in anomaly detection to check the performance gain. Table 5 shows that the refinement strategy can alleviate noise label issues of synthetic data, which makes the detection model more robust.

Table 5. Ablation study for mask refinement. We report averaged detection performances of capsule, transistor, hazelnut, and a wood class of MVTec-AD.

Refinement	Image-level			Pixel-level			
	AUROC	AP	F1	AUROC	AP	F1	AUPRO
×	98.4	99.6	98.4	96.4	80.6	77.4	91.7
○	99.8	100.0	99.7	98.3	80.0	75.4	94.1

5. Conclusion

We propose a diffusion-based defect generation methodology to address data imbalance in anomaly detection. To

improve both the controllability and quality of defect generation, we introduce a masked noising strategy along with a disentanglement loss, which ensures that the background is independent of the defect. Furthermore, we provide theoretical evidence supporting the independence of background denoising and the relationships between the defect latent and masked latent representations.

Based on this theoretical foundation, we show that our methodology outperforms existing approaches in terms of generation quality on benchmark datasets. Our model also helps mitigate the generation of unrealistic defects, which significantly differ from real anomaly instances.

From a generation quality perspective, our synthetic anomaly instances improve anomaly detection performance compared to unsupervised-based methods. Additionally, we demonstrate that these synthetic instances help flatten the loss landscapes, enabling better generalization of the detection model.

Finally, we conduct ablation studies to validate that our regularizer and mask refinement strategies enhance both the quality of defect generation and the robustness of the detection model.

References

- [1] Paul Bergmann, Michael Fauser, David Sattlegger, and Carsten Steger. Mvtec ad—a comprehensive real-world dataset for unsupervised anomaly detection. In *Proceedings of the IEEE/CVF conference on computer vision and pattern recognition*, pages 9592–9600, 2019. 5
- [2] Paul Bergmann, Kilian Batzner, Michael Fauser, David Sattlegger, and Carsten Steger. Beyond dents and scratches: Logical constraints in unsupervised anomaly detection and localization. *International Journal of Computer Vision*, 130(4):947–969, 2022. 5
- [3] Niv Cohen and Yedid Hoshen. Sub-image anomaly detection with deep pyramid correspondences. *arXiv preprint arXiv:2005.02357*, 2020. 2
- [4] Thomas Defard, Aleksandr Setkov, Angelique Loesch, and Romaric Audigier. Padim: a patch distribution modeling framework for anomaly detection and localization. In *International Conference on Pattern Recognition*, pages 475–489. Springer, 2021. 2
- [5] Hanqiu Deng and Xingyu Li. Anomaly detection via reverse distillation from one-class embedding. In *Proceedings of the IEEE/CVF conference on computer vision and pattern recognition*, pages 9737–9746, 2022. 1, 2, 5
- [6] Yuxuan Duan, Yan Hong, Li Niu, and Liqing Zhang. Few-shot defect image generation via defect-aware feature manipulation. In *Proceedings of the AAAI Conference on Artificial Intelligence*, pages 571–578, 2023. 2, 5
- [7] Amir Hertz, Ron Mokady, Jay Tenenbaum, Kfir Aberman, Yael Pritch, and Daniel Cohen-or. Prompt-to-prompt image editing with cross-attention control. In *The Eleventh International Conference on Learning Representations*, 2023. 3
- [8] Martin Heusel, Hubert Ramsauer, Thomas Unterthiner, Bernhard Nessler, and Sepp Hochreiter. Gans trained by a two time-scale update rule converge to a local nash equilibrium. *Advances in neural information processing systems*, 30, 2017. 5
- [9] Jonathan Ho, Ajay Jain, and Pieter Abbeel. Denoising diffusion probabilistic models, 2020. 3
- [10] Teng Hu, Jiangning Zhang, Ran Yi, Yuzhen Du, Xu Chen, Liang Liu, Yabiao Wang, and Chengjie Wang. Anomalydiffusion: Few-shot anomaly image generation with diffusion model. In *Proceedings of the AAAI Conference on Artificial Intelligence*, pages 8526–8534, 2024. 2, 5, 6
- [11] Yiding Jiang, Behnam Neyshabur, Hossein Mobahi, Dilip Krishnan, and Samy Bengio. Fantastic generalization measures and where to find them. *arXiv preprint arXiv:1912.02178*, 2019. 6
- [12] Tero Karras, Samuli Laine, Miika Aittala, Janne Hellsten, Jaakko Lehtinen, and Timo Aila. Analyzing and improving the image quality of stylegan. In *Proceedings of the IEEE/CVF Conference on Computer Vision and Pattern Recognition (CVPR)*, 2020. 2
- [13] Yoon-Yeong Kim, Youngjae Cho, JoonHo Jang, Byeonghu Na, Yeongmin Kim, Kyungwoo Song, Wanmo Kang, and Il-Chul Moon. Saal: sharpness-aware active learning. In *International Conference on Machine Learning*, pages 16424–16440. PMLR, 2023. 6
- [14] Chun-Liang Li, Kihyuk Sohn, Jinsung Yoon, and Tomas Pfister. Cutpaste: Self-supervised learning for anomaly detection and localization. In *Proceedings of the IEEE/CVF conference on computer vision and pattern recognition*, pages 9664–9674, 2021. 2
- [15] Hao Li, Zheng Xu, Gavin Taylor, Christoph Studer, and Tom Goldstein. Visualizing the loss landscape of neural nets. *Advances in neural information processing systems*, 31, 2018. 6
- [16] Dongyun Lin, Yanpeng Cao, Wenbing Zhu, and Yiqun Li. Few-shot defect segmentation leveraging abundant normal training samples through normal background regularization and crop-and-paste operation. *arXiv preprint arXiv:2007.09438*, 2020. 2
- [17] Zhikang Liu, Yiming Zhou, Yuansheng Xu, and Zilei Wang. Simplenet: A simple network for image anomaly detection and localization. In *Proceedings of the IEEE/CVF Conference on Computer Vision and Pattern Recognition*, pages 20402–20411, 2023. 1, 2, 5
- [18] Ron Mokady, Amir Hertz, Kfir Aberman, Yael Pritch, and Daniel Cohen-Or. Null-text inversion for editing real images using guided diffusion models. In *Proceedings of the IEEE/CVF Conference on Computer Vision and Pattern Recognition (CVPR)*, pages 6038–6047, 2023. 3
- [19] Dong Huk Park, Grace Luo, Clayton Toste, Samaneh Azadi, Xihui Liu, Maka Karalashvili, Anna Rohrbach, and Trevor Darrell. Shape-guided diffusion with inside-outside attention. In *Proceedings of the IEEE/CVF Winter Conference on Applications of Computer Vision*, pages 4198–4207, 2024. 4
- [20] Robin Rombach, Andreas Blattmann, Dominik Lorenz, Patrick Esser, and Björn Ommer. High-resolution image synthesis with latent diffusion models. In *Proceedings of the IEEE/CVF Conference on Computer Vision and Pattern Recognition (CVPR)*, pages 10684–10695, 2022. 3
- [21] Robin Rombach, Andreas Blattmann, Dominik Lorenz, Patrick Esser, and Björn Ommer. High-resolution image synthesis with latent diffusion models. In *Proceedings of the IEEE/CVF conference on computer vision and pattern recognition*, pages 10684–10695, 2022. 5
- [22] Olaf Ronneberger, Philipp Fischer, and Thomas Brox. U-net: Convolutional networks for biomedical image segmentation. In *Medical image computing and computer-assisted intervention—MICCAI 2015: 18th international conference, Munich, Germany, October 5-9, 2015, proceedings, part III 18*, pages 234–241. Springer, 2015. 6
- [23] Karsten Roth, Latha Pemula, Joaquin Zepeda, Bernhard Schölkopf, Thomas Brox, and Peter Gehler. Towards total recall in industrial anomaly detection. In *Proceedings of the IEEE/CVF conference on computer vision and pattern recognition*, pages 14318–14328, 2022. 1, 2, 5
- [24] Nataniel Ruiz, Yuanzhen Li, Varun Jampani, Yael Pritch, Michael Rubinstein, and Kfir Aberman. Dreambooth: Fine tuning text-to-image diffusion models for subject-driven generation. In *Proceedings of the IEEE/CVF Conference on Computer Vision and Pattern Recognition (CVPR)*, pages 22500–22510, 2023. 5
- [25] Jiaming Song, Chenlin Meng, and Stefano Ermon. Denois-

- ing diffusion implicit models. In *International Conference on Learning Representations*, 2021. [3](#), [5](#)
- [26] Yang Song, Jascha Sohl-Dickstein, Diederik P Kingma, Abhishek Kumar, Stefano Ermon, and Ben Poole. Score-based generative modeling through stochastic differential equations. In *International Conference on Learning Representations*, 2021. [3](#)
- [27] Richard Zhang, Phillip Isola, Alexei A Efros, Eli Shechtman, and Oliver Wang. The unreasonable effectiveness of deep features as a perceptual metric. In *Proceedings of the IEEE conference on computer vision and pattern recognition*, pages 586–595, 2018. [5](#)